TEN MICRON SPECTROSCOPY OF YOUNG STARS IN THE ρ OPH CLOUD

M.S. Hanner, T.Y. Brooke[a]

MS 169--237, Jet Propulsion Laboratory, California institute. of Technology

4800 Oak Grove Dr., Pasadena, CA, 91109

and

A.T. Tokunaga

Institute for Astronomy, University of Hawaii

2680 Woodlawn D., Honolulu, 11196822

[a]NAS/NRC Resident Research Associate.

ABSTRACT

Spectra in the 10 μm region were obtained of 14 young stars associated with the ρ Oph dark C1OU d. Silicate dust emission and absorption features can be fairly well reproduced with simple models using the emissivity of the silicates in the Orion Trapezium region, believed to be typical of molecular cloud dust. A spectrum of the Trapezium star θ^1 Ori D was obtained to define this emissivity more precisely. The emissivity of silicate dust around the late - type giant μ Cep does not improve the fits to the absorption features and provides a poorer match to the emission features, None of the sources display a strong 11.25 μm peak like that seen in comet Halley and attributed to crystalline olivine. A broad shallow feature near 11.25 μm, possibly related to the comet feature, is evident in the emission spectrum of the Ae star HD J 50193. Absorption features toward two of the objects are narrower than would be expected from Trapezium - like silicates, suggesting differences in the composition of the silicates. The relation between the silicate extinction band depth and H_2O ice band depths is determined for the deeply embedded objects. One late – type object, Elias 14, clearly shows the 11.25 μm aromatic hydrocarbon emission feature., possibly excited by the nearby B star, HD 147889, though the latter dots not exhibit the feature.

1. INTRODUCTION

Many young stars have silicate dust emission or absorption features at 10 μm. The spectral shape of the. 10 μm Si–O band reflects the mineralogy of the. silicate.s. Oxygen- rich late -- type stars and proto–planetary nebulae show a rich variety of mineralogies indicative of the temperature and pressure. conditions in circumstellar regions (e.g. Barlow 1993). It is usually assumed, based on the available spectra, that silicates around young stars have. the broad, structureless shape peaking around 9.7 μm seen in molecular clouds: the "Trapezium" profile (Gillett *et al.* 1975; Whittet *et al.* 1988). The Trapezium emissivity is generally attributed to amorphous silicates (e.g. Day 1974; Dorschner *et al.* 1988). However, narrower emission features attributed to more crystalline. silicates have been reported around a few young stars, such as AB Aur (Cohen and Witteborn 198S).

Silicates in comets, however, appear to have quite different spectra] shapes from that of the. Trapezium (see Hanner *et al.* 1994 for a review). Comets are believed to have formed in regions of the primitive solar nebula that were. cold enough for inte.]-stellar grains to have been incorporated directly with little. alteration. But a sharp spectra] peak at 1 J.2 μm, attributed to crystalline olivine, has been seen in at least three comets, including P/Halley (Bregman *et al.* 1 987; Campins and Ryan 1989; Hanner *et al.* 1990: Lynch *et al.* 1992.). Could cometary grains have been annealed by heating in the solar nebula during the sun's T Tauri phase? If so, then one might expect to see evidence of annealing in the silicate. dust around young stellar objects. Aitken *et al.* (1988) reported a weak 11.2 μm feature in absorption along the line of sight to GL 2591 which they attributed to crystalline. silicates.

The current generation of infrared array spectrometers makes it possible. to determine the spectra] shapes of the silicate features of young stars with improved sensitivity and spectra] resolution over previous groundbased surveys (e.g. Cohen and Witteborn 1985) and IRAS LRS spectra.

'l'he. nearby ρ Ophiuchus cloud contains numerous young stellar objects, including precursors of solar mass stars (e.g. Lada and Wilking 1984), making it an ideal region to conduct a survey. In this paper we. report observations of 14 objects in the. central core of the *p Oph* cloud, selected from the lists of Elias (1978) and Wilking and Lada (1983). Our primary objective was to determine the. spectral shapes of the silicate. emission and absorption bands for comparison to cometary silicate emission. We have modelled each spectrum assuming a Trapezium - like emissivity, then searched for deviations from this profile. For absorption features, the extinction band depths due to silicates along the line--of – sight were also estimated.

2. OBSERVATIONS

The spectra of the p Oph objects were. obtained at the United Kingdom Infrared Telescope (UKIRT) on UT 29 May 1991 ant] 23, 24 June 1992. The 32– element grating spectrometer CGS3 was used in the low resolution mode, giving a spectral resolution of approximately SS. Data were obtained through a 5.5" aperture, usually at two grating positions approximately 1/2 resolution element apart. "The sky chopping throw was 15" EW in 1991 and ?,0" EW in 1992. Wavelength calibration was determined by observing the emission lines in the planetary nebula NGC 6572; we estimate the uncertainty to be $\pm$ 0.03 μm.

Sources were observed at airmass 1.4--2.0. Repeated spectra of β Oph (K2 III) were used to define an atmospheric extinction correction at each wavelength and each source spectrum was corrected to unit air mass. The flux standard was α Lyr, assumed to be a 9600 K blackbody with flux 1.17 X 10^{-12} Wm^{-2} μm^{-1} at 10.1 μm (Rieke *et al.* 1985).

On UT 4 Nov 1993, a spectrum of the Orion Trapezium star θ^1 Ori D was obtained with CGS3 at the same resolution. A 9.4" aperture was used. This region contains extended 10 μm emission (e.g. Gehrz *et al.* 1975). The sky chopping throw was set to 90″ EW to minimize contamination in the reference beam. The airmass standard was α Tau; the flux standard was α CMa, assumed to be a 10000 K blackbody with flux 4.33 x 10^{-12} Wm^{-2} μm^{-1} at 10.1 μm.

The sources are listed in Table 1 and their spectra are plotted in Figs. 1-4. An additional object, WL16, is described in Hanner, Tokunaga, and Geballe (1992). For objects with fluxes $\lesssim 10^{-13}$ Wm^{-2} μm^{-1} the spectra were smoothed with a triangle function of FWHM= 0.2 μm to improve the signal – to– noise. The effective resolution of these spectra is $\approx$ 0.28 μm.

3. A NEW TRAPEZIUM EMISSIVITY SPECTRUM

Interstellar silicate features are often compared to the "Trapezium" emissivity obtained from a spectrum of the strong silicate emission feature in the Orion Trapezium H II region by assuming optically thin emission at a single temperature, 250 K (Forrest *et al.* 1975; Gillett *et al.* 1975). To define this emissivity more. precisely, we observed the Trapezium star θ^1 Ori D as described above.. 'l'he data are shown in Fig. 1a.

The. overall shape of the. θ^1 Ori D spectrum matches the. Forrest *et al.* data reasonably well. However, forbidden lines of Ar III at 8.99 pm, S IV at 10.51 μm and Ne II at 12.81 pm, and an emission feature at 11.25 μm can be. seen in our spectrum at spectral resolu t ion R ~55. A spectrum of this feature taken with CGS3 at a resolution of ~190 shows it to have. the. characteristic width and shape of the 11.25 μm aromatic hydrocarbon emission feat ure. We removed the. forbidden lines by linear interpolation. To remove. the contribu ticm of the hydrocarbon bands at 7.7, 8.6, and 11.25 μm, we assumed that their spectral shape was the same. as that seen in the Orion bar (Bregman *et al.* 1989; Roche *et al.* 1989), scaled to fit the Trapezium flux near 11.25 pm, as shown in Fig. la.

The resulting relative emissivity obtained by subtracting the features and dividing by a 2S0 K blackbody is shown in Fig. lb. 'l'his profile. is similar to the. broad, structureless silicate emission feature given by Gillett *et al. (1975),* Possible. structure between 9.7 and 10 μm is uncertain due. to the possibility of incomplete correction for the. strong telluric ozone. absorption in this region. We compare the new Trapezium emissivity to the. spectra of the. ρ Oph objects, in the following section.

4. MODEL FITS TO THE SPECTRA

Determining the spectral emissivity of the silicates from observations requires knowing the optical depths of all of the. dust components which contribute to the. 10

μm spectrum. This is a difficult challenge., beyond the scope of this paper, requiring knowledge of the densities, temperatures, and dust geometries (e.g. disks or spherical enve.lope.s) aroun d each object. It is clear, for example., that the. silicate. emission features of Fig. 2 are. not due solely to optically thin emission from Trapezium - like silicates, since. the. feature. contrasts are lower than that of Fig. lb. Dilution by featureless emission or optical depth effects could account for the lower contrast.

Accordingly, we have. taken the approach of applying simple. models to test how well each spectrum can be reproduced by assuming that the. grains producing the. feat ure have. the Trapezium emissivity, $\varepsilon_t(\lambda)$, given in Fig. lb. We. modeled the spectra in four limiting cases described below. The underlying continuum emission in each source was assumed to follow a power law in wave length. The use of power]aws rather than single – temperatur e. blat.kbodies is motivated by the. success of models which include grains at a range. of temperatures to match the. spectral energy distributions of young stars (e.g. Adams *et al.* 1987; Hillenbrand *et al.* 1993). The models given here c1o not incorporate any specific geometries for the dust; more. detailed modeling of the. entire. spectral energy distributions would be required to constrain the dust spatial distributions. The goal here is to see whether some. simple modeling can reproduce the observed range. of 8 – 13 μm spectra with a given emissivity.

Emission features were modelled with cases 1 – 3 and absorption features with cases 3 and 4, described below. For each spectrum, a least squares minimization was performed to determine best- fit values for the parameters: i.e. the optical depths, spectral indices, and normalization factors.

Case 1 -- Variable optical depth (after Cohen and Witteborn 198S)

$$\lambda F_\lambda = a_0(\frac{\lambda}{9.7})^m (1 - e^{-a_1\epsilon_t(\lambda)}) \qquad (1)$$

With $\epsilon_t(\lambda)$ normalized at 9.7 μm, the. parameter a_1 is the total silicate optical depth at 9.7 μm, $\tau_{9.7}$. This slab model approximates a dusty envelope. which both emits and absorbs at 10 μm.

Case 2 – Two component: Optically **thick** + optically thin **emission**

$$\lambda F_\lambda = a_0(\frac{\lambda}{9.7})^n + a_2(\frac{\lambda}{9.7})^m \epsilon_t(\lambda) \qquad (2)$$

The quantity $f = a_2/(a_0 + a_2)$ is the. relative. contribution of the. optically thin grains to the flux at 9.7 μm. This model might apply, for example, to an optically thin envelope and an optically thick disk (or the. star itself), both of which both Contribute to the flux at 10 μm. The optically thick component could alternatively represent emission from featureless dust,

Case 3 - Optically **thin with** line of sight extinction (after Gillett *et al.* 1975)

$$\lambda F_\lambda = a_0(\frac{\lambda}{9.7})^m \epsilon_t(\lambda) e^{-a_1\epsilon_t(\lambda)} \qquad (3)$$

The parameter a_1 is equal to the. total line. of sight extinction at 9.7 pm, $\tau_{9.7}$. Note, that both the emitting ant] the absorbing groins are. assumed to have. the. Trapezium emissivity. This equation might apply to an optically thin circumstellar envelope. obscured by cold dust along the line of sight.

Case *4* - Optically thick with line of sight extinction

$$\lambda F_\lambda = a_0\left(\frac{\lambda}{9.7}\right)^{m} e^{-a_1 \tau_i(\lambda)} \qquad (4)$$

The parameter a_1 is the total line. of sight extinction at 9.7 μm, $\tau_{9.7}$. This equation might apply to an optically thick disk or envelope (or the star itself) obscured by cold dust.

The best-fit parameters for each case are given in Tables 2 and 3 and the fits plotted in Figs. 2 and 3. Fits to the emission features with case 3 were very similar to those of case 1 and are not plotted,

The silicate optical depths derived under case 3 refer to the extinction by cold (non -- emitting) dust along the line of sight. If the extinction is interstellar, so that the extinction of the. star and the. dust envelope are the same, then it is likely that the derived optical depths are too high, given the estimated visual extinctions, A_v, to these stars. For an extinction law typical of dust in the solar neighborhood, $A_V/\tau_{9.7}$ - 18.5 (Roche and Aitken 1984), the required A_v values for HD 150193, Elias 28, and Elias 13 under case 3 would be 9.6, 13, and 19, respective.ly, compared to previously estimated values of 1.S, 4.5, and 2.2 (1 Iillenbrand *et al.* 1993; Cohen and Kuhi 1979; Bouvier and Appenzeller 1992). Although the extinction laws to the.se. stars are not known precisely, this tends to favor either model 1 or 2 to explain the observe.cl emission features. Foɪ mode.] 1 to avoid the same objection as model 3, the. geometry **must be.** such that the. extinction of the star is only a small fraction of the extinction in the dust envelope.

The main l-e.suit is that all of the. silicate features can be fairly well matched by the Tɪ apezium emissivity using one or more models, with some possible deviations noted below. For the emission features, adoption of a variable optical depth (e.g. Cohen and Witteborn 1985) is not necessarily required. Such a model does reproduce the. HD 1S0193 spectrum well, but a two– component model provides a comparably good fit to Elias 28. Thus, the observed contrast in the silicate. emission featuɪ e. does not necessarily provide a direct measure of the. silicate optical depth, since an optically thick compon en t will lower the contrast.

For the. absorption features, the optically thick model with extinction (case 4) reproduced the. data fairly well. Optically thin **emission** with **extinction** (case 3) improves the fit at the bottom of the band in all cases (especially WL 12, Elias 21) but requires the flux to drop sharply at 8 μm, which is not consistent with the data. This is because the. exponential extinction affects the wave.] engths near the. peak of the band more. strongly than the. wings. Gillett *et al.* (1975) found that including optically thin emission did impɪ eve. the. fits to the silicate absorption features toward deeply embedded H II regions.

WC. also investigated whether the narɪ ower, more. symmetric, silicate. emissivity seen around the. late–type giant μ Cep (Roche and Aitken 1984) would provide betteɪ fits to the young stars. Roche and Aitken suggested that silicate. dust in the diffuse interstellar medium is more consistent with the μ Cep emissivity. We found that the. agreement was never better than the. Trapezium models. For the strong emission features in HD 150193 and Elias 28, models with the μ Cep profile were significantly worse. (e.g. Fig. 5a). For the. absorption features, no reasonable fits could be found using the. μ Cep profile. with case 3; fits using case 4 were generally of comparable quality to those obtained with the Trapezium emissivity (e.g. Fig. 5b). Whittet *et* al. (1988) found that the. Trapezium gave a better match than μ Cep to silicate. emission and absorption features in the region of the Taurus dark cloud.

Thus the silicates along the. lines of sight to these young stars in the. ρ Oph cloud generally appear to be. similar to Trapezium silicates. With the. possible exceptions discussed below, there does not appear to be structure, in the. silicate. spectrum. in particular, none. of the. spectra show a prominent 11.2 μm feature. similar to that observed in Comet Halley and attributed to crystalline. olivine (Bregman *et* al. 1987; Campins and Ryan 1989). This implies either that substantial thermal annealing of the. silicates has not yet occurred in the. cloud or that, if thermal annealing has taken place close. to the stars, the. annealed grains are concealed by optically thick shells.

5. DEVIATIONS FROM THE TRAPEZIUM EMISSIVITY

5.1 HD 150193

Although none of cmr sources display a *strong* 11.2 μm peak like that seen in Comet Halley, excess emission near 11.25 μm at the. 10 percent level is evident on the wing of the strong emission feature. in the. Ae star HD 1S0193. A similar emission feature. at 11.25 μm may be present in Elias 28 and Elias 13 but the. lower signal/noise. in these spectra makes its reality uncertain. For 1111150193, the feature appears to be broader than the typical aromatic hydrocarbon emission band at 11.25 μm (FWHM - 0.2.- 0.4 μm; Witteborn *et al.* 1989, Roche *et al.* 1991) and there is no evidence of emission from the related hydrocarbon 8.6 μm feature or the. wing of the. 7.7 μm feature. Yet HD 150193 is a Herbig Ae/Be star (Finkenzeller and Mundt 1984) and it is not unusual for such stars to exhibit emission from the. hydrocarbon bands (Brooke *et al.* 1993), Brooke *et al.* (1 993) did not detect the. aromatic 3.2.9 μm feature in HD 150193 and placed an upper limit to the 3.29 μm feature flux of 0.8 x 10^{-15} Wm^{-2}. Based on a typical flux ratio of the. 1 1 .25/3 .29 bands of -2-4 (Puget and Leger 1989), the 11.25 μm aromatic emission could contribute., at most, only about half of the. excess flux at 11.25 pm, although this flux ratio varies substantially from object to object (Cohen *et al.* 1989). Observations at higher spectral resolution are needed to clarify the possible contribution of aromatics and better define. any new silicate feature in HD 150193.

There *is* a dip near 9.8 μm in the. spectrum of 111>150193, producing an apparent maximum in the. silicate emissivity at around 9.4 **pm. No strong aromatic** features lie in this region, The dip occurs in the. region of strong telluric ozone absorption but, if real, the peak at 9.4 μm could indicate. a compositional difference in the silicates around this star,

5.2 Absorption Features

There appear to be significant deviations from the Trapezium emissivity in two of the absorption sources; both Elias 21 and W]. 12 require a silicate emissivity that is narrower than that of the. Trapezium. To illustrate this, the. parameters for the Case 4 fits were used to invert the. data and obtain new relative emissivity profiles. This procedure is valid as long as the true emissivities do not differ greatly from the Trapezium emissivity and the. model assumptions are correct. The derived emissivities normalized roughly to the.ir peaks are. shown with the Trapezium emissivity normalized in the same way in Fig. 6. Elias 2.1 and WL 12 have. similar profiles that are. lower than the Trapezium on the long wavelength side. This narrower profile could indicate. differences in the. composition of the. silicates. These two objects have the. coolest dust continuum emission of any sources in our sample.. The wavelength of maximum and the. width of the central part of the. feature are. similar to the. μ Cep emissivity although the wings differ.

Cohen & Witteborn (198S) concluded that a few young stars, such as the Herbig Ae/Be star AB Aur, had silicate. emission features narrower than expected from the Trapezium emissivity; they attributed this to more. crystalline. silicates. in contrast to Elias 21 and W]., 12, AB Aur matches the. Trapezium on the long wavelength side, but requires a narrower emissivity on the short wavelength side, so different materials appear to be. involved.

Both crystalline and amorphous silicates can differ in the width and the wavelength of maximum of their 10 μm spectral feature. (see discussion in Hanner *et* al. 1994). Amorphous olivine (e.g. Stephens and Russell 1979) and amorphous pyroxenes (e.g. Dorschner *et al.* 1988) have both been suggested as plausible candidates to explain the Trapezium emissivity, the. pyroxenes tending to peak at shorter wavelengths compared to olivine (see. also Day 1979; Krätschmer and

I luff man 1979). Ncme of the samples measured in theses papers displays a 10 μm feature wide enough to explain the Trapezium emissivity by itself, assuming grain radii < 0.S μm. Some of the amorphous materials do have features wide enough to match a narrower feature like those seen toward Elias 21, WI, 12 or AB Aur, though we have not found a precise. spectra] match. Koike and Hasegawa (1987) suggest that the width of the 10 μm feature in amorphous silicates is correlated with the $Si0_2$ content, with higher SiO_2 content leading to progressively narrower features peaking at shorter wavelengths. Thus compositional differences within amorphous silicates may be sufficient to explain the deviations from the Trapezium emissivity seen in a few young stars, without the need for invoking a higher degree of crystallinity.

A change in the mean particle size can also affect the width of the 10 μm silicate feature; larger particles cause the feature to broaden on the. long wavelength side. This effect is significant for particles with radii $\gtrsim$ 0.75 pm, larger than the canonical value for interstellar grains (Draine and Lee 1984). Note also that the grains in the Trapezium would have to be the larger ones,

6. SILICATE ANI> H_2O ICE BAND DEPTHS

Our models provide estimates of the extinction due to silicate grains toward the young stars in the ρ Oph cloud under different assumptions. The extinction due to silicates can be compared to the extinction at other wavelengths to determine the. broad optical properties of the grains along the line of sight. Values of the total visual extinction, A_v, are difficult to estimate for the deeply embedded objects.

These objects do exhibit 3 μm H_2O ice absorption bands, however. Thus we limit the discussion to a comparison of the. silicate. and H_2O ice band depths.

A major uncertainty in the estimation of the. silicate band extinction depths towards the embedded sources is the possibility of intrinsic silicate emission in the sources. Our two models give. good upper and lower limits to the extinction. in the limit that the intrinsic emission is optically thin (case. 3), the derived optical depths are greater by - 2, compared to the optically thick model (case 4). As discussed above, the model which included optically thin emission did not in general provide better fits to the spectra compared to the model with extinction only, (see Fig. 2 and Table 3). Also, if there were optically thin emission, the extinction were interstellar (so that the. star suffers the same extinction as the emitting dust), and the extinction law were similar to that in the solar neighborhood, $A_V/\tau_{9.7}$ - 18.5 (Roche and Aitken 1984), then the implied A_v values for the visible stars Elias 22, Elias 30, Elias 16, and 111>147889 would be. extremely high: 31, 44, 27, and 42 mag, respectively, compared to previously estimated values for these stars of 6.6, 5,0, 6.2, and 4.6 mag (Bouvier and Appenzeller 1992; Adams *et al.* 1987; Elias 1978). The implied A_v values for the optically thick case are closer to the. literature values, though only upper limits can be obtained for Elias 22 and Elias 16. For these reasons, we will assume. in this section that there is no significant silicate emission in the embedded sou rces.

Figure 7 shows the H_2O ice band optical depth, $\tau_{3.08}$ from Tanaka *et* al. (1990), plotted against the silicate band optical depth for the. *p* Oph sources in which both features were detected. There is rough correlation, though with considerable scatter; a formal weighted fit gives:

$$\tau_{3.08} = 1.06 \pm 0.04(\tau_{9.7} - 0.004 \pm 0.021). \tag{5}$$

It would be useful to compare this relation to the results for embedded young stars in other clouds. The. slope is a measure. of the extent of ice mantling on grains; a negative, intercept could indicate an extinction threshold above which H_2O ice is shielded from destruction by the interstellar or circumstellar radiation field (cf Whittet *et al.* 1988). Whittet *et al.* obtained ice and silicate optical depths for four embedded young stars in the Taurus cloud assuming no intrinsic silicate emission in the sources, but the data show too much scatter to define any clear relation at this time. They also obtained data for field stars behind the Taurus cloud, but there is at this time insufficient data to say definitively whether the. $\tau_{3.08}$ vs. $\tau_{9.7}$ relation for the ρ Oph embedded objects is significantly different from the relation for the Taurus field stars.

Note that even a small amount of intrinsic emission would tend to shift the points to the right on Fig. 7, rendering conclusions about the slope and threshold of the $\tau_{3.08}$ vs. $\tau_{9.7}$ relation somewhat uncertain. Further progress in the determination of this relation for the *p Oph* cloud will come from better observations of the absorption band depths in background stars free of circumstellar dust.

7. AROMATIC HYDROCARBON EMISSION FEATURES IN ELIAS 14

The spectrum of Elias 14 is plotted in Fig. 4. An emission peak at 11.25 μm is clearly visible, with a width ~ 0.4 μm, consistent with the 11.25 μm aromatic hydrocarbon feature (see. e.g. Roche *et al.* 1991). The rising slope near 8 μm is consistent with the presence of the 7.7 μm feature, but the expected 8.6 μm feature, if present at all, is weak. Elias 14 is the. second young stellar object with strong aromatic emission features we have found in the ρ Oph cloud; the first was WL 16 (Hanner et *al.* 1992). Both sources exhibit plateau emission longward of the 11.25 μm feature, but there is no clear evidence for the 12.7 μm feature seen in WL 16 in the Elias 14 spectrum.

The presence of aromatic hydrocarbon emission feature.s in Elias 14 is surprising since the spectral type. of this object is estimate.d to be K0 (Bouvier and Appenzeller 1993), and the family of aromatic emission features is usually seen in regions of high ultraviolet flux (for a recent review, see Sellgren 1990). Furthermore, the star does not show a significant dust excess in groundbased photometry; the infrared colors up to 10 μm are consistent with a reddened photosphere (Lada and Wilking 1984). However, Elias 14 lies only about 10′ away (projected distance 0.5 pc for a distance. d = 160 pc) from the B2 V star HD 147889, and in the region of extended IRAS 12 μm emission excited by this star (Greene and Young 1989). So it seems plausible that the B star excites the feature in the dust around Elias 14. Interestingly, HD 147889 itself does not show any evidence of the 11.25 μm feature (Fig. 2), perhaps due. to destruction or dehydrogenation of the aromatics near the star.

Two stars with silicate absorption features (Elias 23 and Elias 30) also appear to have some excess emission at 11.25 μm, though the cancellation of the sky background is poor in each case. Elias 23 also lies in the region of strong 12 μm emission around HD 147889 (as does Elias 21); Elias 30 lies just outside. this region. Both are classified as KO (Bouvier and Appenzeller 1993; Chini 1981).

8. CONCLUSIONS

1. Silicate emission and absorption features toward young stars in the ρ Oph cloud can be fairly well represented by the. Trapezium silicate dust emissivity common in molecular clouds using simple. models. This indicates that substantial thermal annealing of the. silicates along the lines of sight has not occurred. If thermal annealing has taken place close to the stars, spectral signatures of the. annealed grains are masked by optically thick shells. The emissivity of the dust around the late– type giant μ Cep does not provide significantly better fits to the absorption sources and provides a poorer match to the emission sources,

2. "There are possible deviations from the Trapezium emissivity in some objects, which could indicate differences in silicate composition. The strong silicate emission feature in the Herbig Ae/Be star HD1 50193 shows deviations at the. 10% level from the Trapezium emissivity at 9.4– 10 μm and near 11.25 μm. Narrower silicate features are seen in absorption toward two objects, Elias 21 and WL. 12.

3. Silicate extinction band depths were estimated for the deeply embedded sources. The slope of the $\tau_{3.08}$ vs. $\tau_{9.7}$ relation was estimated (assuming no intrinsic silicate emission in the sources).

4. At least one KO star in the. c1ouc1, Elias 14, shows the 11.25 μm emission feature due to aromatic hydrocarbons, probably excited by the nearby B2 V star, HD 147889.

ACKNOWLEDGEMENTS

We thank the staff of the [JK11{'1' and Joint Astronomy Centre for their support. UKIRT is operated by the. Royal Observatory Edinburgh on behalf of the U.K. Science and Engineerin g Research Council. A portion of this research was carried out at the Jet Propulsion Laboratory, California Institute of Technology under contract with the National Aeronautics and Space Administration. A. Tokunaga acknowledges support of NASA Grant NAGW–2278. T. Brooke acknowledges a postdoctoral fellowship from the. National Research Council.

REFERENCES

Adams, F. C., Lada, C. J., and Shu, F. 11.1987, ApJ 312, 788.

Aitken, D. K., Roche, P. F., Smith, C. H., James, S. D., and Hough, J. 11.1988, MNRAS, 230, 629.

Barlow, M. J. 1993, in Astronomical Infrared Spectroscopy: Future Observational Directions, ed. S, Kwok, Vol 41, Astronomical Society of the Pacific Conference Series, p. 97.

Bouvier, J. and Appenzeller, I. 1992, Astr. Ap. Supp. 92, 481.

Bregman, J. D., Allamandola, L. J., Tielens, A. G. G. M., Geballe, T. R., and Witteborn, F. C. 1989, ApJ 344, 791.

Bregman, J. D., Campins, H., Witteborn, F. C., Wooden, D. H., Rank, D. M., Allamandola, L. J., Cohen, M., and Tielens, A. G. G. M. 1987, Astr. Ap. 187, 616.

Brooke, T. Y., Tokunaga, A. T., and Strom, S. E. 1993, AJ 106, 656.

Campins, H. and Ryan, E. V. 1989, Ap.J. 341, 1059.

Chini, R. 1981, Astr. Ap. 99, 346.

Cohen, M., and Kuhi, L. V. 1979, ApJS, 41, 743.

Cohen, M., and Tielens, A. G. G. M., Bregman, J., Witteborn, F. C., Rank, D., Allamandola, L. J., Wooden, D. H., and de Muizon, M. 1989, ApJ 341, 246.

Cohen, M., and Witteborn, F. C. 1985, ApJ, 294, 345.

Day, K, L. 1974, ApJ 192, L15.

Day, K. L. 1979, ApJ 234, 158.

Dorschner, J., Friedemann, C., Gurtler, J. and Henning, T. 1988, A&A, 198, 223.

Draine, B. T. and Lee, H. M. 1984, ApJ 285, 89.

Elias, J. H. 1978, ApJ, 224, 453.

Finkenzeller, U. and Mundt, R. 1984, Astr. Ap. Supp. S5, 109,

Forrest, W. J., Gillett, F. C., ant] Stein, W. A. 1975, ApJ, 195, 423.

Gehrz, R. D., Hackwell, J. A., and Smith, J. R. 1975, ApJ 202, 1.33.

Gillett, F. C., Forrest, W. J., Merrill, K. M., Capps, R. W., and Soifer, B. T. 1975, ApJ, 200, 609.

Greene, T. P., and Young, E. T. 1989, ApJ, 339, 258.

Hanner, M. S., Lynch, D. K., and Russell, R. W. 1994, ApJ, in press,

Hanner, M. S., Newburn, R. 1.., Gehrz, R. D., Harrison, T., Ney, E. P., and Hayward, T. I.. 1990, ApJ, 348, 312.

Hanner, M. S., Tokunaga, A. T., and Geballe, T. R. 1992, ApJ, 395, 1.111.

Hillenbrand, 1., A., Strom, S. E., Vrba, l?. J., ant] Keene, J. 1993, ApJ 397, 613.

Koike, C. and Hasegawa, 11.1987, Ap.Sp. Sci. 134, 361.

Krätschmer, W. and Huffman, D. R. 1979, Ap. Sp. Sci. 61, 195.

Lada, C. J., and Wilking, B. A. 1984, ApJ, 287, 610.

Lynch, D. K., Russell, R. W., Hackwell, J. A., Hanner, M. S., and Hammel, H. B. 1992, Icarus, 100, 197.

Puget, J. 1,., and Leger, A. 1989, ARA&A 27, 161.

Rieke, G. H., Lebofsky, M. J., and Low, F. J. 1985, AJ, 90, 900,

Roche, P. F., and Aitken, D. K. 1984, MNRAS, 208, 481.

Roche, P. F., Aitken, D. K., and Smith, C.H. 1989, MNRAS, 236, 485.

Roche, P. F'., Aitken, D. K., and Smith, C. 11.1991, MNRAS, 252, 282.

Sellgren, K. 1990, in Dusty objects in the Universe, ed. E. Bussoletti and A.A. Vittone (Kluwer, Dordrecht), p. 35.

Smith, R. S., Sellgren, K., and Brooke, '1', Y. 1993, MNRAS, 263, 749.

Stephens, J. R. and Russell, R.W. 1979, ApJ, 228, 780.

Tanaka, M., Suto, S., Nagata, T., and Yamamoto, T. 1990, ApJ, 352, 724.

Whittet, D. C.B., Bode, M. F., Longmore, A. J., Adamson, A. J., McFadzean, A. D., Aitken, D. K., and Roche, P. F. 1988, MNRAS, 233, 321.

Wilking, 13, A., and Lada, C. J. 1983, ApJ, 274, 698.

Witteborn, F. C., Sandford, S. A., Bregman, J. D., Allamandola, L. J., Cohen, M., Wooden, D. H., and Graps, A. L. 1989, ApJ, 341, 270.

FIGURE CAPTIONS

Fig. 1 –(a) Spectra of the Orion Trapezium star θ^1 Ori D obtained with the UKIRT CGS3 low resolution grating through a 9.4" aperture. Dashed line is the scaled Orion bar aromatic hydrocarbon spectrum. (b) Relative. emissivity found by linearly interpolating under the emission features, subtracting the component due to aromatic hydrocarbons, and dividing by a 250 K blackbody. 'l'he relative emissivity has been smoothed by a triangle function of FWHM =0.2 μm and normalized at 9.7 μm.

Fig. 2(a – c) – Spectra of ρ Oph sources with silicate emission features obtained with the UKIRT CGS3 low resolution grating through a S.5" aperture.. Model fits are. described in the text.

Fig. 3(a – j) – Spectra of p Oph sources with silicate absorption features obtained with the UKIRT CGS3 low resolution grating through a 5.5" aperture. Mode.] fits are described in the text,

Fig. 4 –Spectrum of Elias 14 in the ρ Oph cloud obtained with the UKIRT CGS3 low resolution grating in 1992 through a 5.5" aperture..

Fig. 5– (a) Fits to HD 150193 using the μ Cep emissivity profile. (b) Fit to Elias 21 using the μ Cep emissivit y profile..

Fig. 6–Resulting emissivities of Elias 21 and WL 12 after inverting a fit with extinction only (case 4). The emissivities have been normalized roughly to their peaks.

Fig. 7-~ H_2O ice band optical depths from Tanaka *et al.* (1990) plotted against silicate. absorption band depths for deeply embedded ρ Oph sources, assuming no intrinsic silicate emission. Dashed line is the best least squares fit.

TABLE 1

Log of the Observations

	Date (UT)	Integration Time (min)
HD 147889 (Elias 9)	5/29/1991	6.7
Elias 13		20
Elias 14		20
Elias 16		20
Miss 21		2.7
Elias 22		5.3
Elias 23		5.3
Elias 28		5.3
Elias 29		2
Elias 30		5.3
HD 150193 (Elias 49)		3,3
Elias 14	6/23/1992	40
Elias 24		13.4
Elias 33	6/24/1992	8
WL 12		12
0^1 Ori D	11/4/1993	4

TABLE 2

Fit Parameters for ρ Oph Emission Features[a]

	Case 1 Variable optical depth				Case 2 Two component					Case 3 Opt. thin w/extinction			
	a_0^b	m	$\tau_{9.7}$	χ^2_ν	a_0^b	n	a_2^b	m	χ^2_ν	a_0^b	m	$\tau_{9.7}$	χ^2_ν
HD 150193	100.2	-1.10	1.18	21.5	13.5	-2.4	58.2	-0.43	34.8	115.9	-1.10	0.52	20.6
	(1.1)	(0.01)	(0.02)		(0.3)	(0.2)	(0.4)	(0.06)		(0.6)	(0.01)	(0.01)	
Elias 28	7.6	-0.11	1.73	2.3	1.3	-3.4	5.1	1.6	1.4	12.6	-0.11	0.70	2.3
	(0.3)	(0.06)	(0.12)		(0.3)	(1.3)	(0.3)	(0.2)		(0.4)	(0.06)	(0.04)	
Elias 13	2.7	-0.27	2.97	1.8	1.0	-2.3	1.6	2.1	1.3	7.1	-0.29	1.04	1.8
	(0.1)	(0.09)	0.26)		(0.2)	(1.2)	(0.2)	(0.5)		(0.3)	(0.09)	(0.06)	

[a]Errors in parentheses.

[b]Units are 10^{-3} Wm^{-2}.

TABLE 3

Fit Parameters for ρ Oph Absorption Features

	Case 3 opt, thin w/extinction				Case 4 Opt. thick w/extinction			
	a_0^a	m	$\tau_{9.7}$	χ_ν^2	a_0^a	m	$\tau_{9.7}$	χ_ν^2
Elias 29	796.4	-0.83	3.38	43.2	146.6	-0.67	1.51	10.5
	(4.2)	(0.01)	(0.01)		(0.7)	(0.01)	(0.01)	
WL 12	52.8	0.55	3.06	7.6	9.4	0.69	1.15	4.1
	(0.8)	(0.03)	(0.03)		(0.1)	(0.03)	(0.03)	
Elias 33	39.8	-1.14	2.17	4.6	7.6	-0.97	0.36	1.8
	(0.7)	(0.04)	(0.03)		(0.1)	(0.04)	(0.03)	
Miss 21	194.5	1.36	2.40	7.9	36.9	1.52	0.61	8.6
	(1.6)	(0.02)	(0,01)		(0.3)	(0.02)	(0.01)	
Elias 24	26.1	-0.86	1.87	3.2	5.0	-0.65	0.10	1.7
	(0.6)	(0.05)	(0.03)		(0.1)	(0.05)	(0.03)	
Elias 23	39.8	-0.95	2.03	2.1	7.6	-0.75	0.26	2.2
	(0.6)	(0.03)	(0,03)		(0.1)	(0.03)	(0.02)	
Elias 22	41.2	-1.22	1.68	4.5	8.3	-1.01	0.0	2.5
	(0.5)	(0.03)	(0.02)		(0.1)	(0,03)	(0.02)	
Elias 30	36.2	-1.18	2.36	4.8	6.8	-1.01	0.54	2.6
	(0.8)	(0.05)	(0.04)		(0.1)	(0.04)	(0.03)	
Elias 16	3.9	-1.37	1.48	3.1	0.91	-1.38	0.0	2.8
	(0.4)	(0,24)	(0.14)		(0.03)	(0.21)	(0.14)	
HD 147889	16.9	-2.81	2.31	1.5	3.0	-2.55	0.43	1.2
	(1.5)	(0,21)	(0.15)		(0.2)	(0,20)	(0.14)	

^{a}Units are 10^{-13} Wm^{-2}.

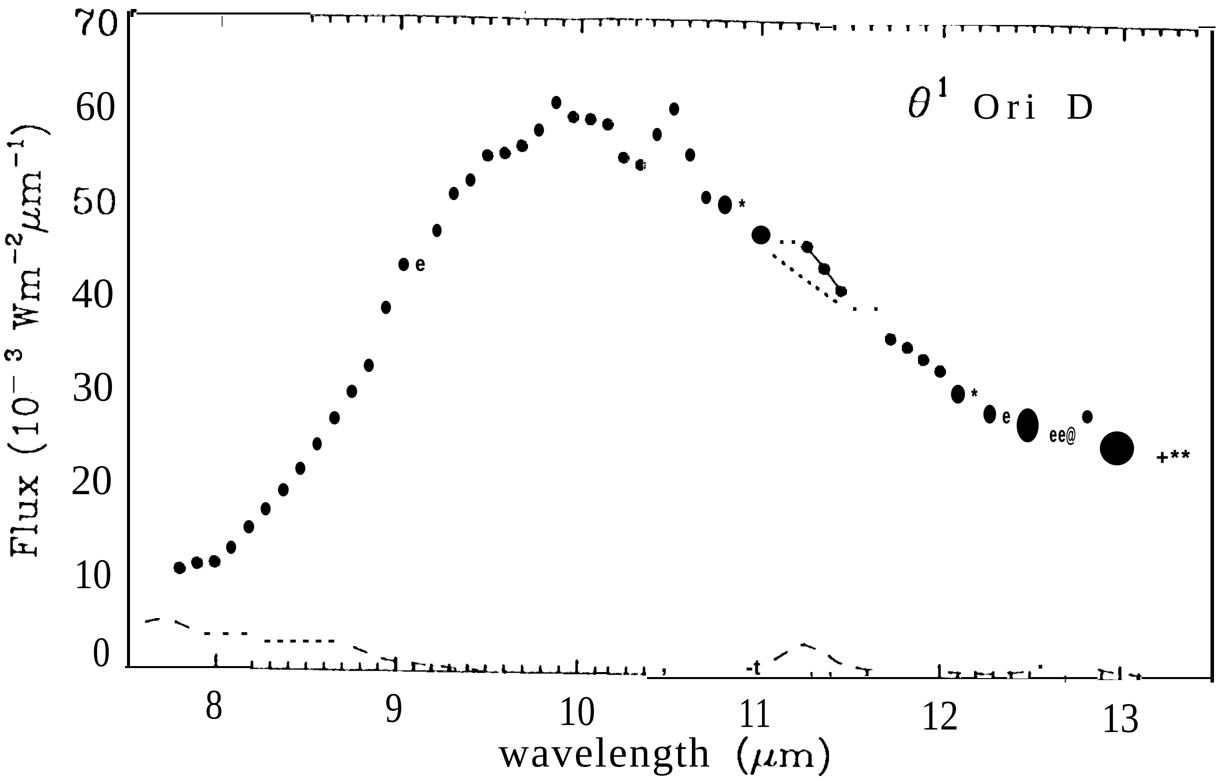

θ^1 Ori D
Flux (10^{-3} W m^{-2} μm^{-1})
wavelength (μm)

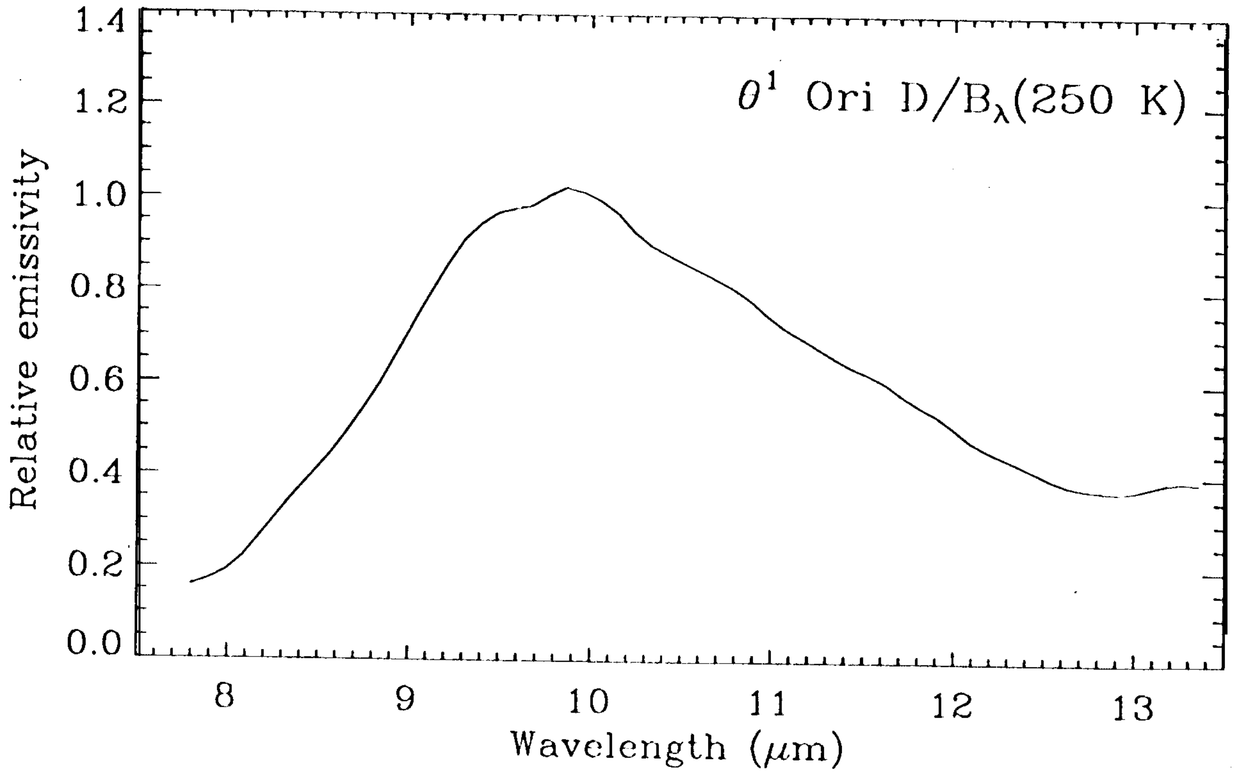

θ^1 Ori D/B_λ(250 K)
Relative emissivity
Wavelength (μm)

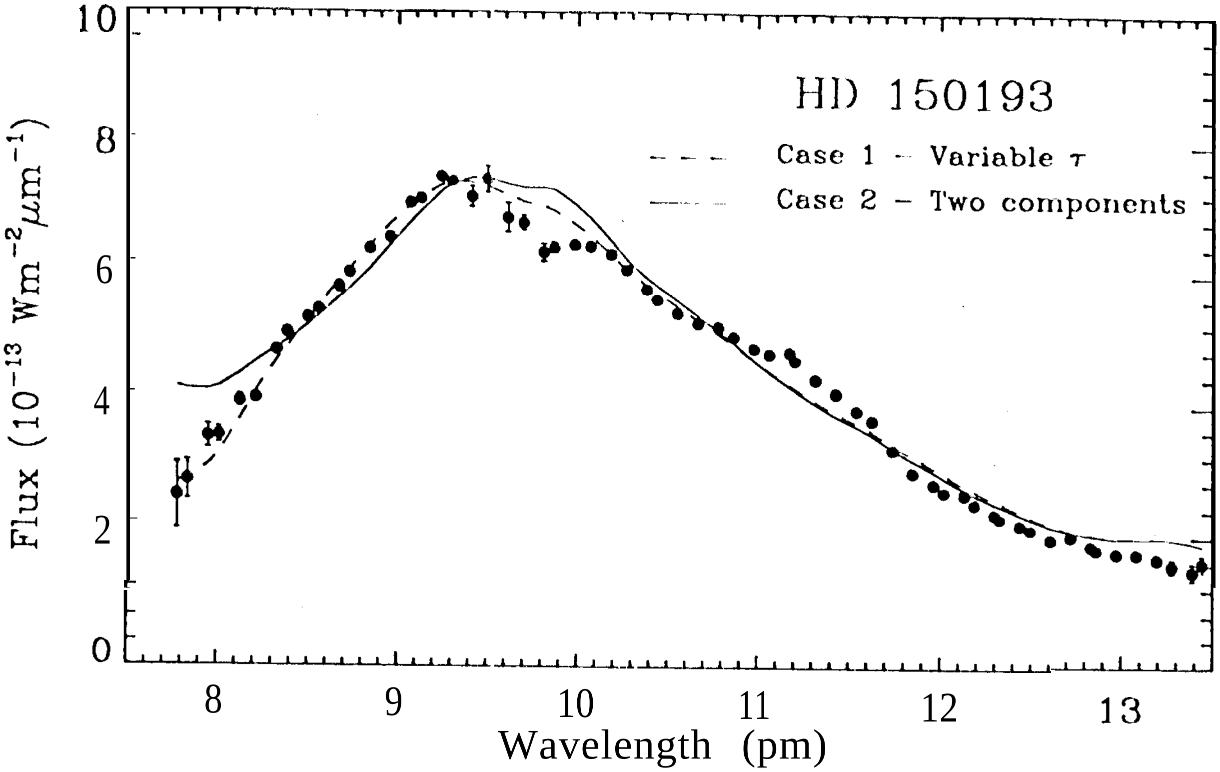

HD 150193
Case 1 - Variable τ
Case 2 - Two components
Flux (10^{-13} Wm^{-2}μm^{-1})
Wavelength (pm)

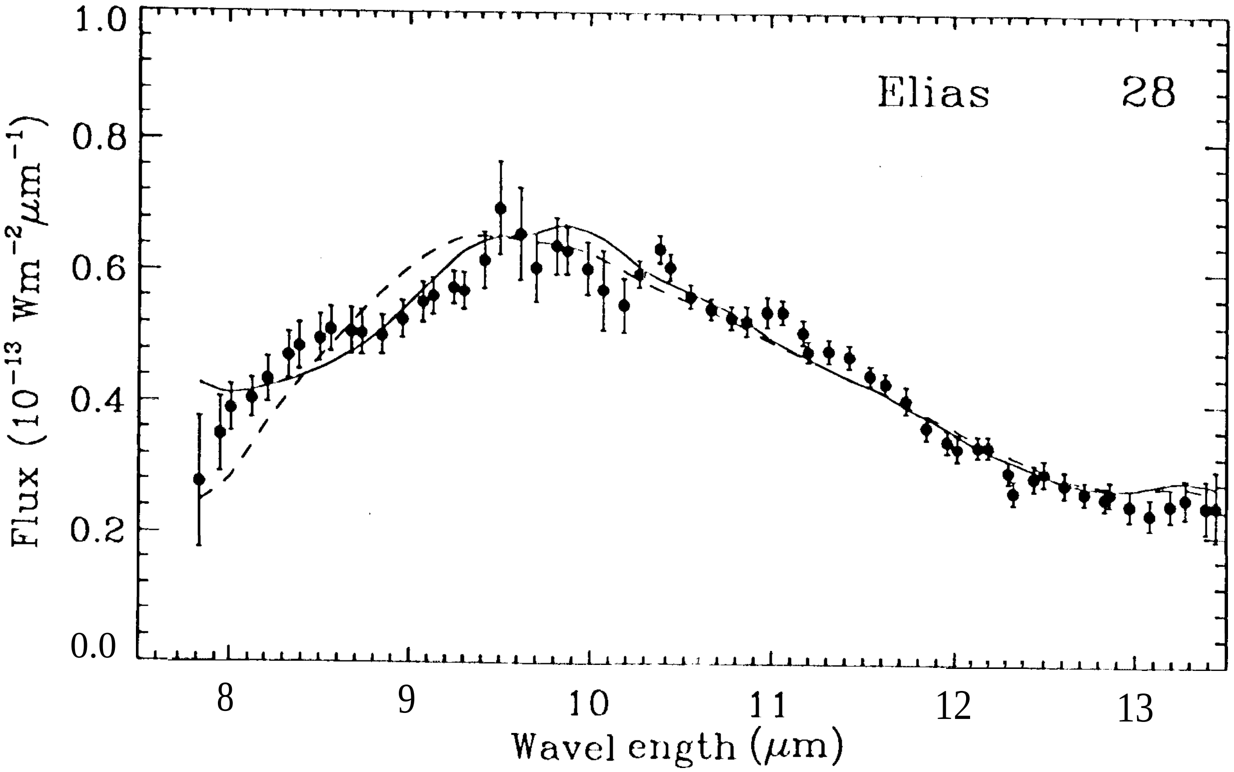

Elias 28
Flux (10^{-13} Wm^{-2}μm^{-1})
Wavel ength (μm)

Fig 8a 8b

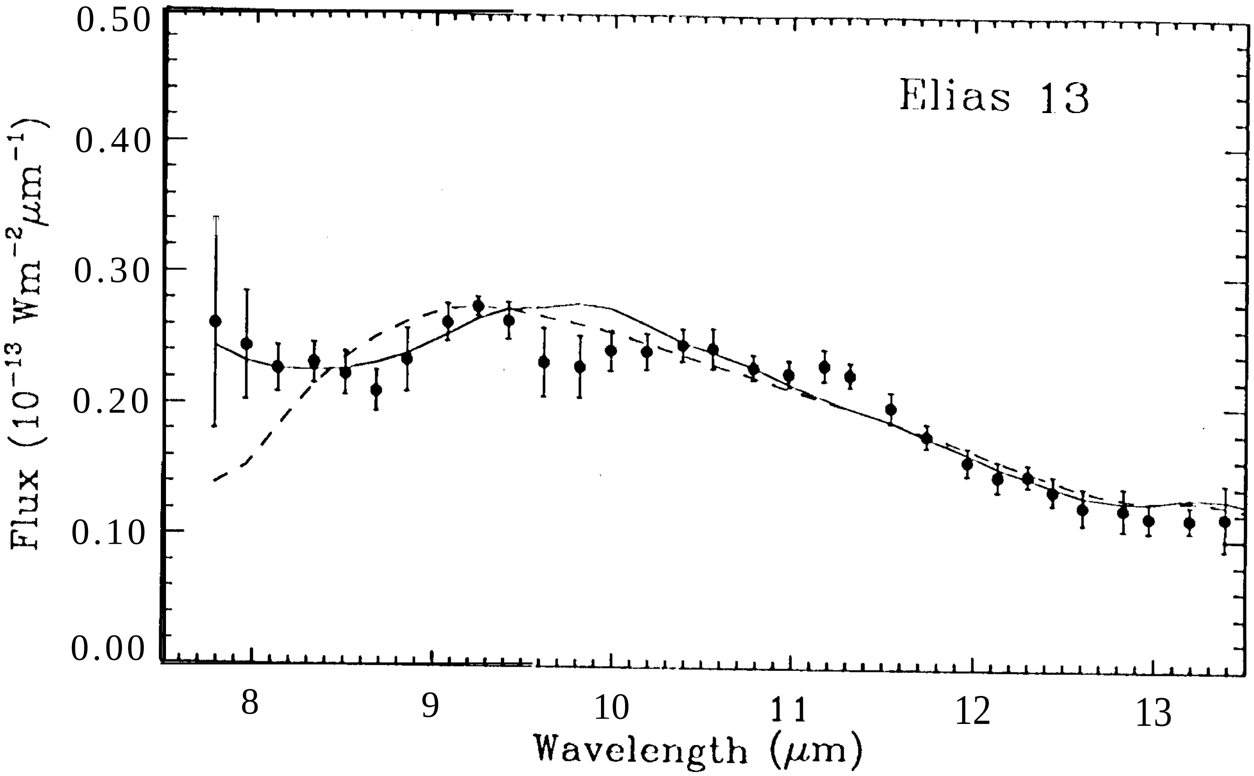
Elias 13
Flux (10^{-13} Wm$^{-2}\mu$m^{-1})
0.50
0.40
0.30
0.20
0.10
0.00
8
9
10
11
12
13
Wavelength (μm)

Fig. 2c

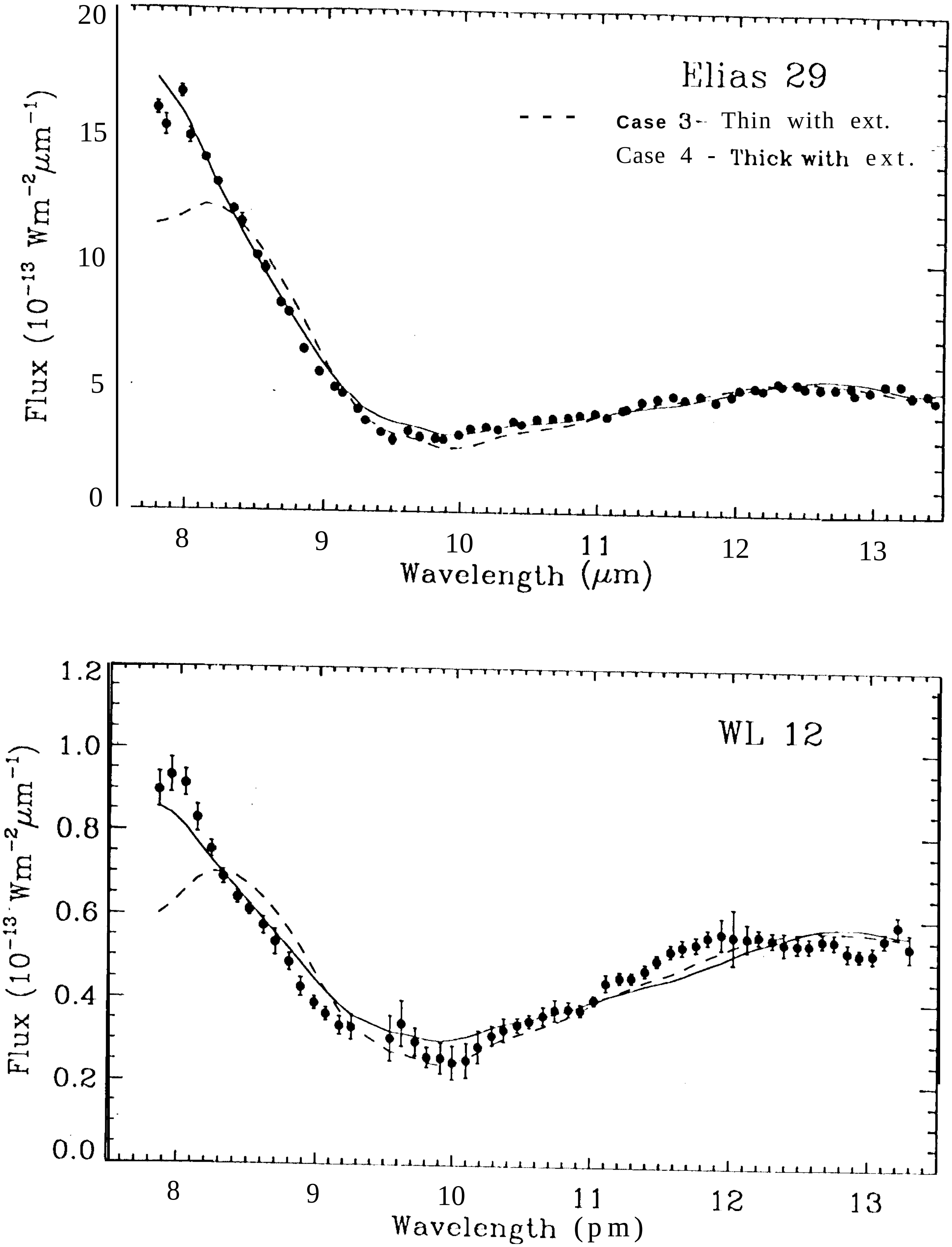
Elias 29
Case 3 - Thin with ext.
Case 4 - Thick with ext.
Flux (10^{-13} Wm$^{-2}\mu$m^{-1})
Wavelength (μm)
WL 12
Flux (10^{-13} Wm$^{-2}\mu$m^{-1})
Wavelength (pm)

Fig. 3a, 3b

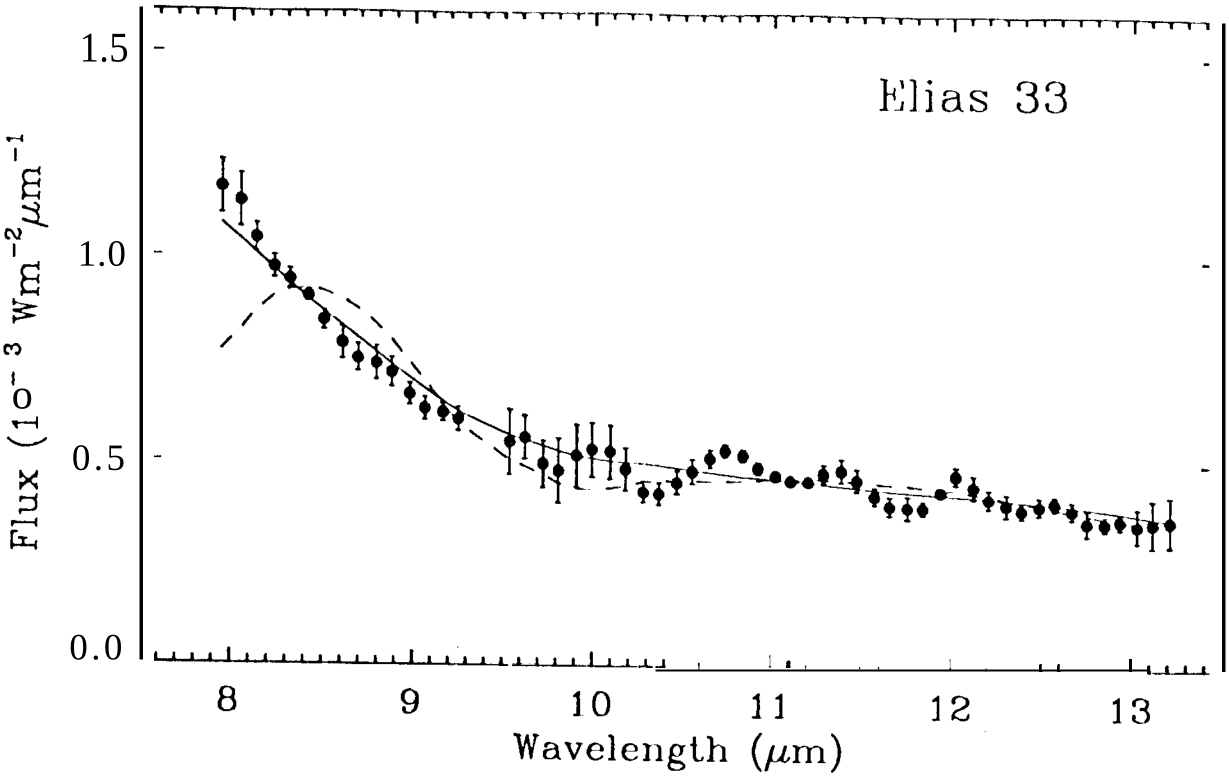

Elias 33
Flux (10^{-3} Wm$^{-2}\mu$m^{-1})
1.5
1.0
0.5
0.0
8
9
10
11
12
13
Wavelength (μm)

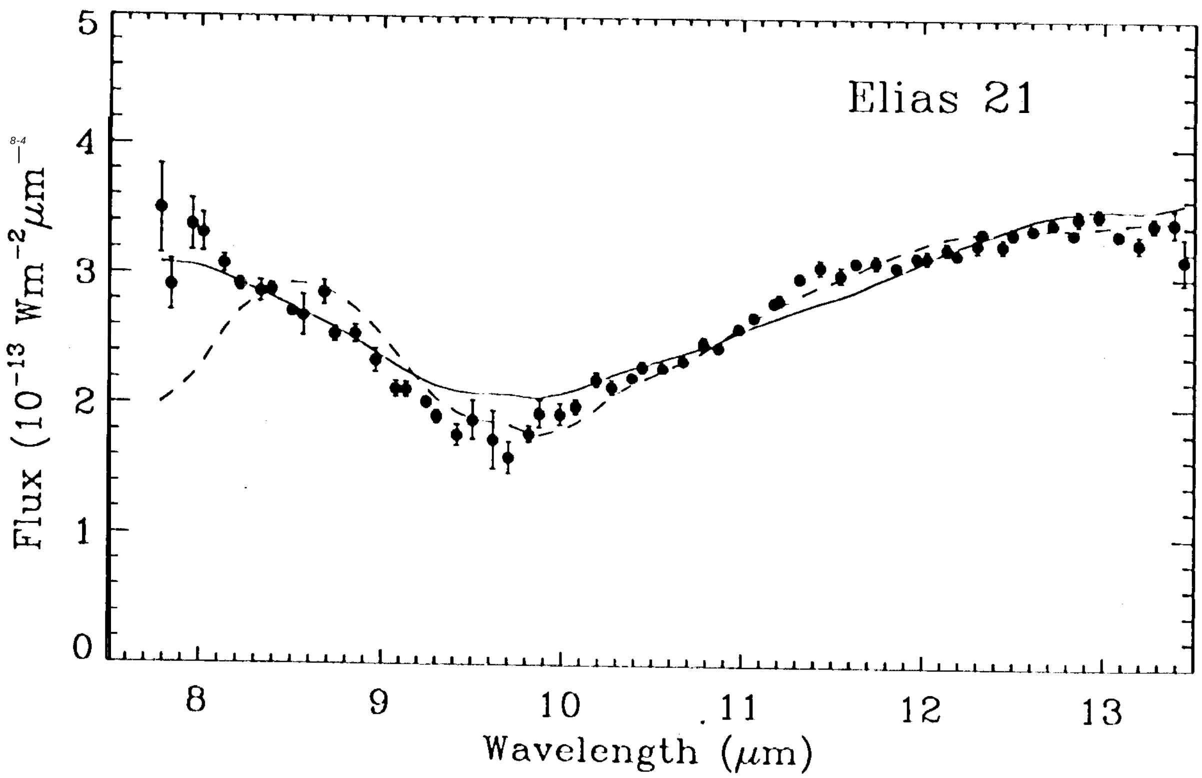

Elias 21
Flux (10^{-13} Wm$^{-2}\mu$m^{-1})
5
4
3
2
1
0
8
9
10
11
12
13
Wavelength (μm)

Fig. 5 5d

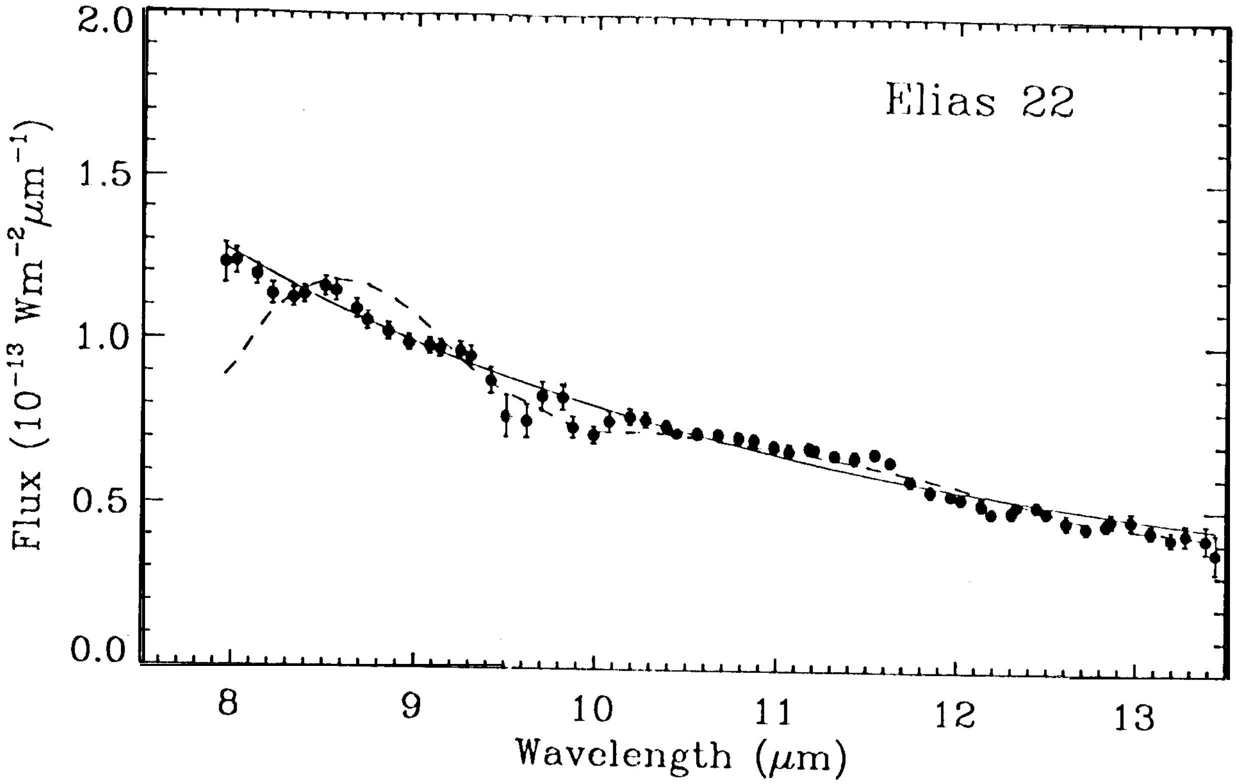
Elias 22
Flux (10^{-13} Wm$^{-2}\mu$m^{-1})
Wavelength (μm)
2.0
1.5
1.0
0.5
0.0
8
9
10
11
12
13

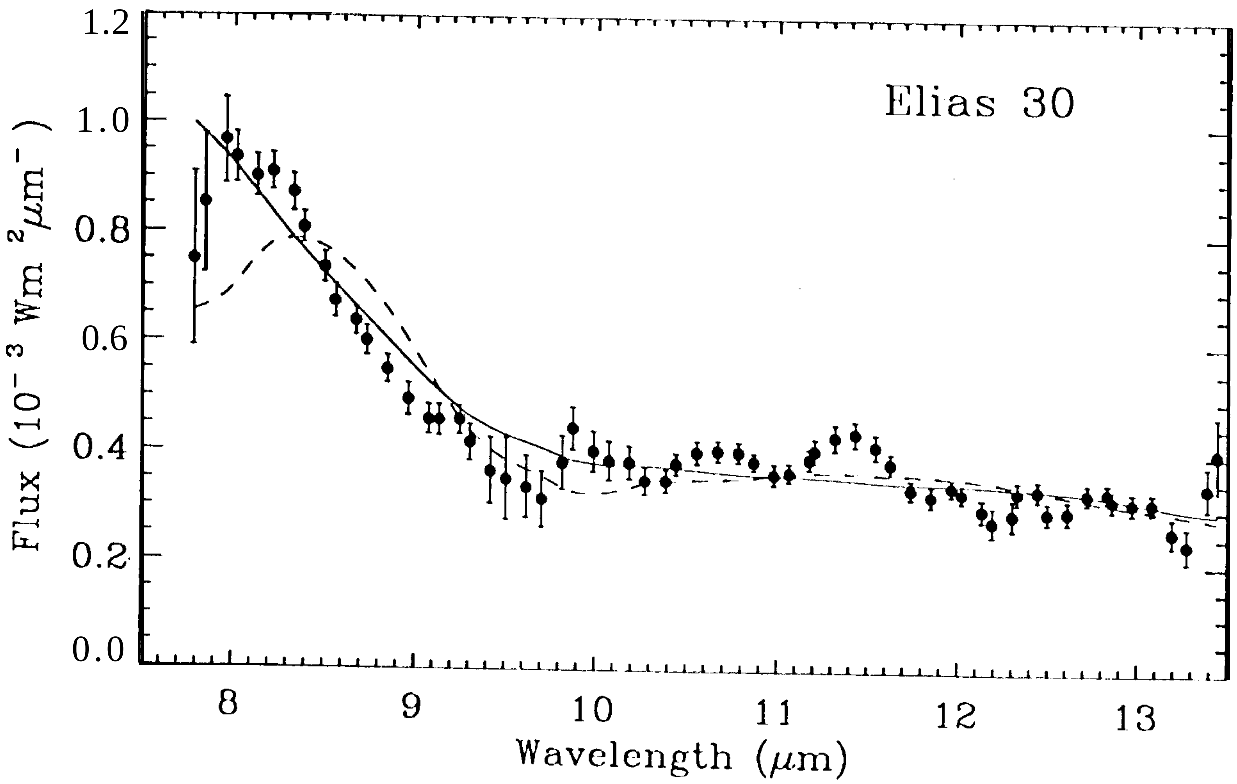
Elias 30
Flux (10^{-3} Wm $^{2}\mu$m^{-})
Wavelength (μm)
1.2
1.0
0.8
0.6
0.4
0.2
0.0
8
9
10
11
12
13

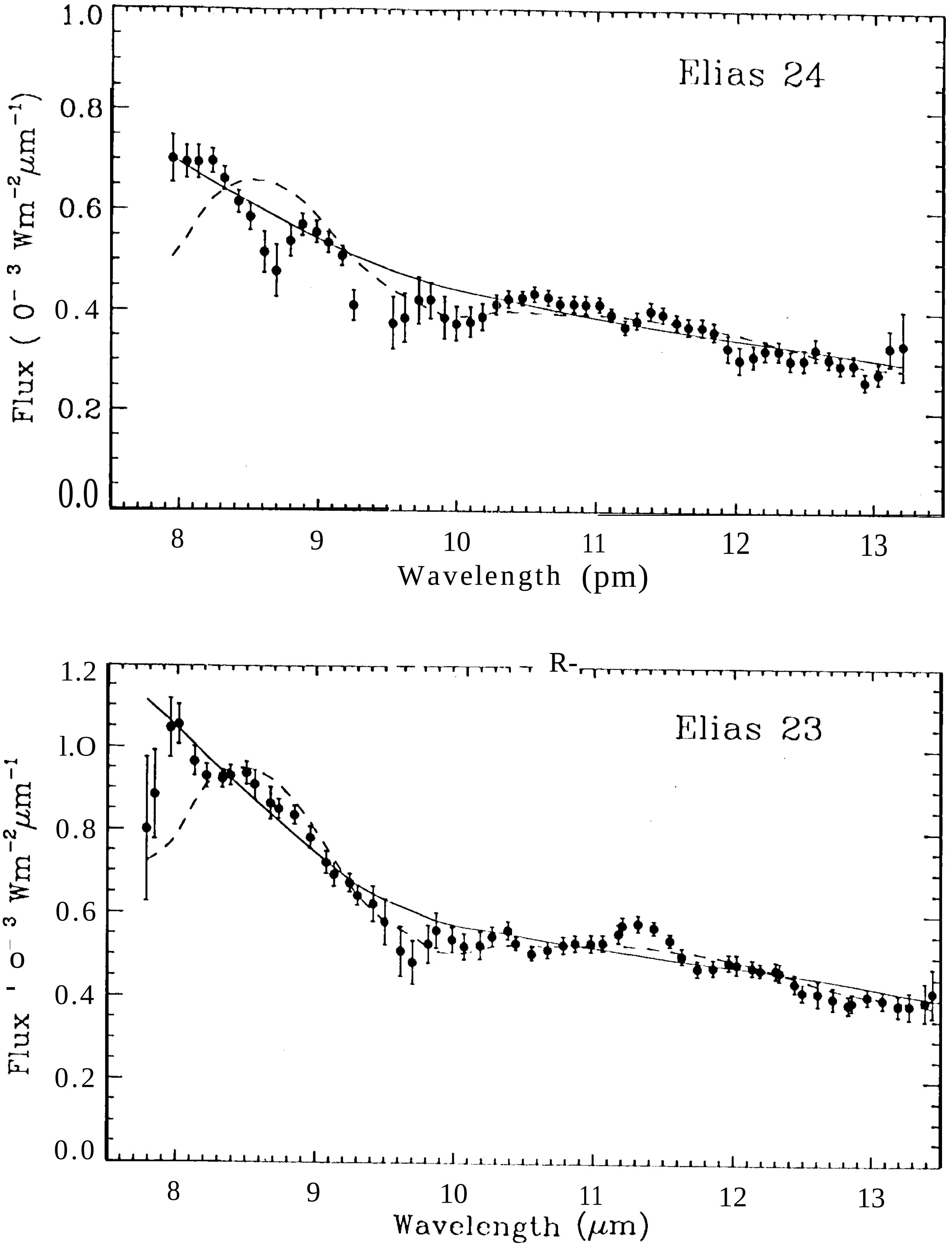

Elias 24
Flux (0⁻ 3 Wm⁻²μm⁻¹)
1.0
0.8
0.6
0.4
0.2
0.0
8
9
10
11
12
13
Wavelength (pm)
Elias 23
R-
Flux ' o⁻ 3 Wm⁻²μm⁻¹
1.2
1.O
0.8
0.6
0.4
0.2
0.0
8
9
10
11
12
13
Wavelength (μm)

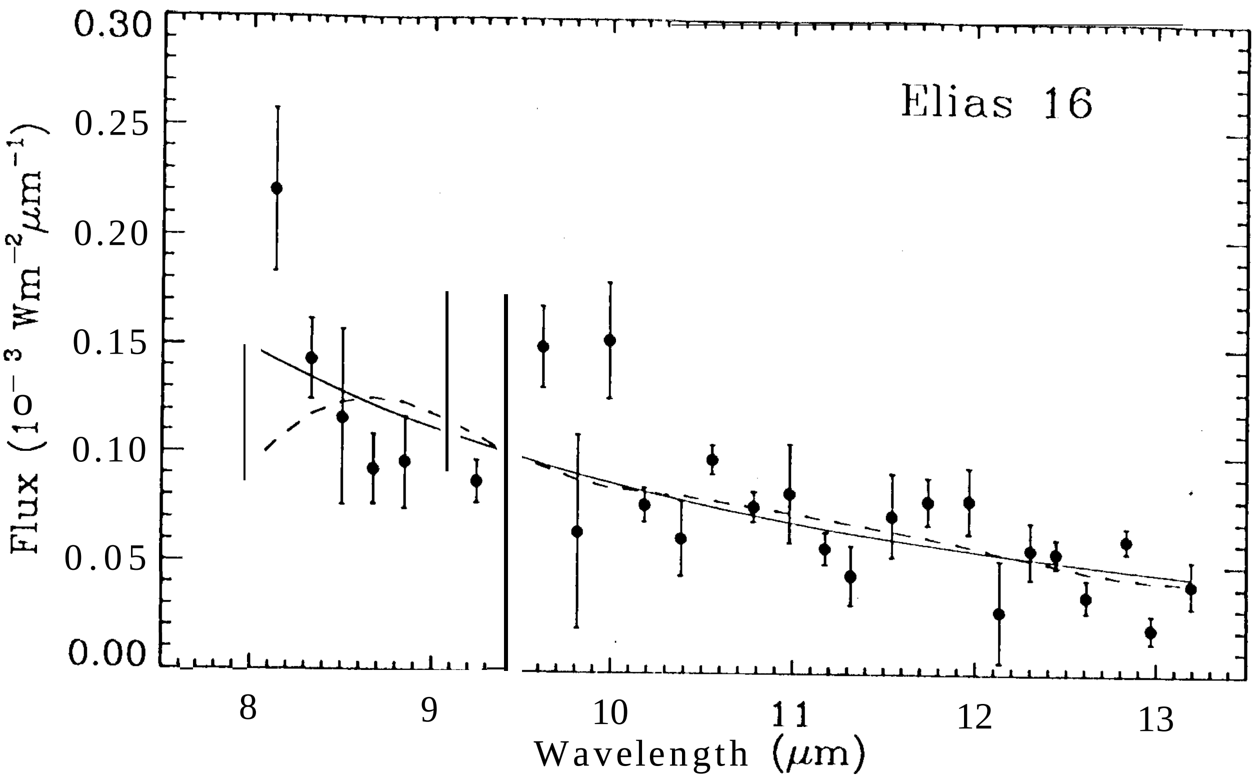
Elias 16
Flux (10^{-3} Wm^{-2}μm^{-1})
0.30
0.25
0.20
0.15
0.10
0.05
0.00
8
9
10
11
12
13
Wavelength (μm)

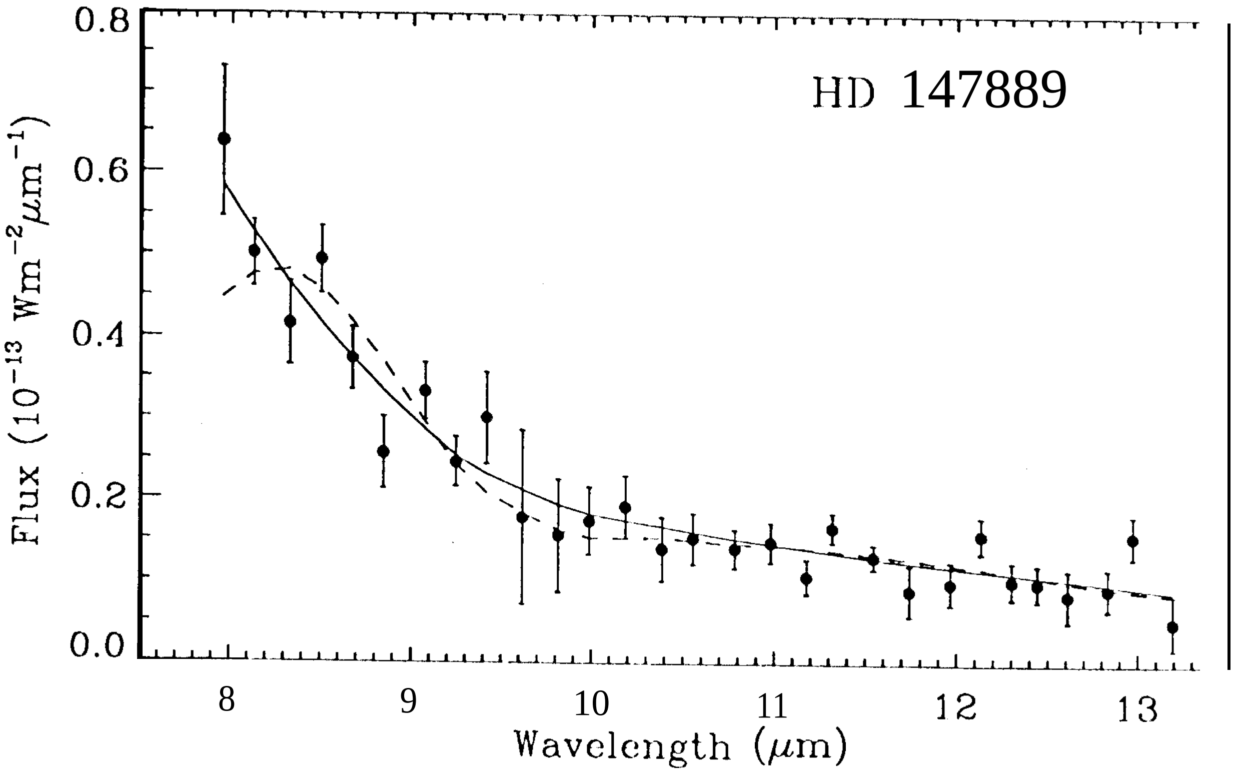
HD 147889
Flux (10^{-13} Wm^{-2}μm^{-1})
0.8
0.6
0.4
0.2
0.0
8
9
10
11
12
13
Wavelength (μm)

Fig. 3a

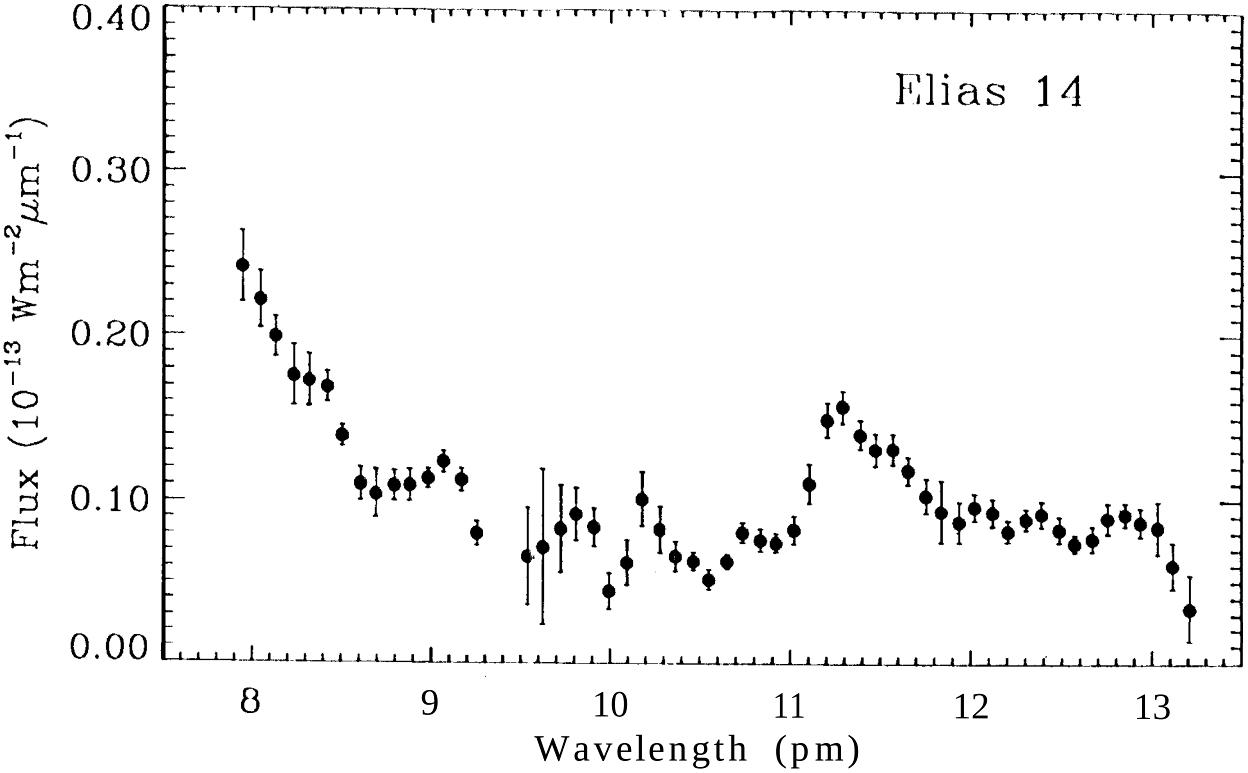

Elias 14
Flux $(10^{-13}\ Wm^{-2}\mu m^{-1})$
0.00
0.10
0.20
0.30
0.40
8
9
10
11
12
13
Wavelength (pm)

Fig. 4

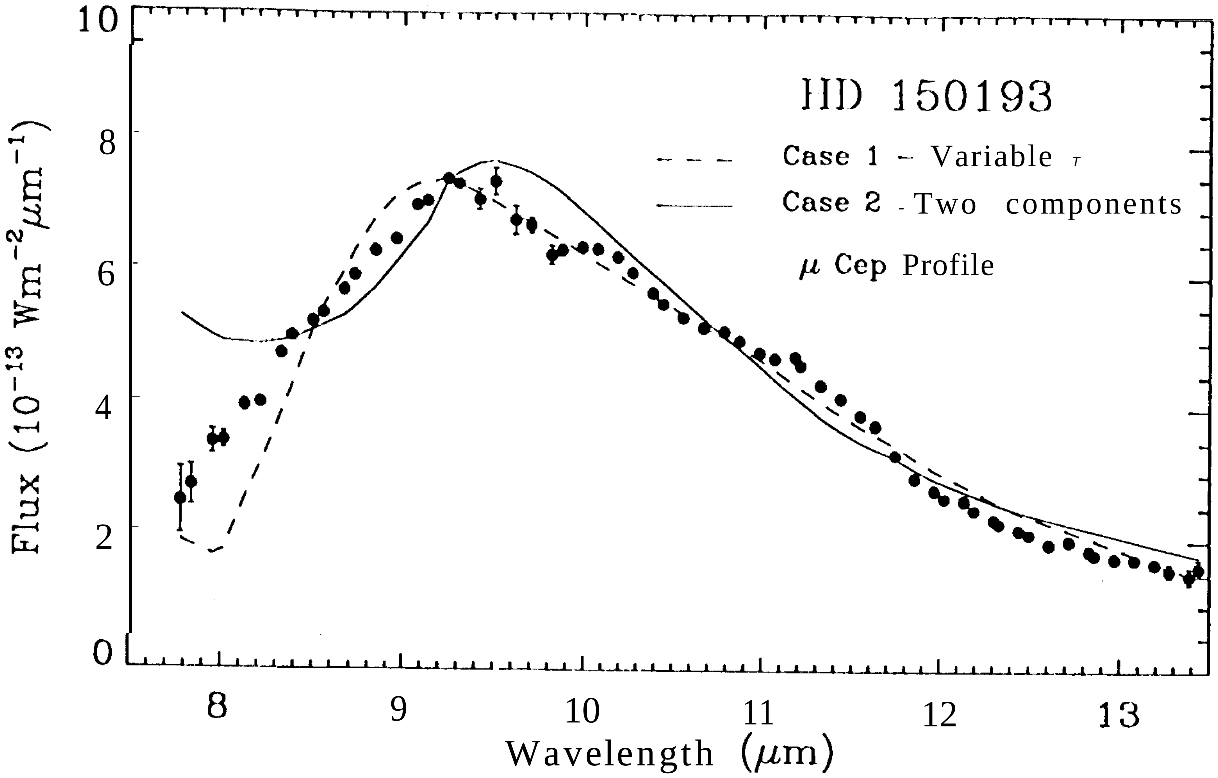
HD 150193
Case 1 - Variable τ
Case 2 - Two components
μ Cep Profile
Flux (10^{-13} Wm^{-2}μm^{-1})
Wavelength (μm)

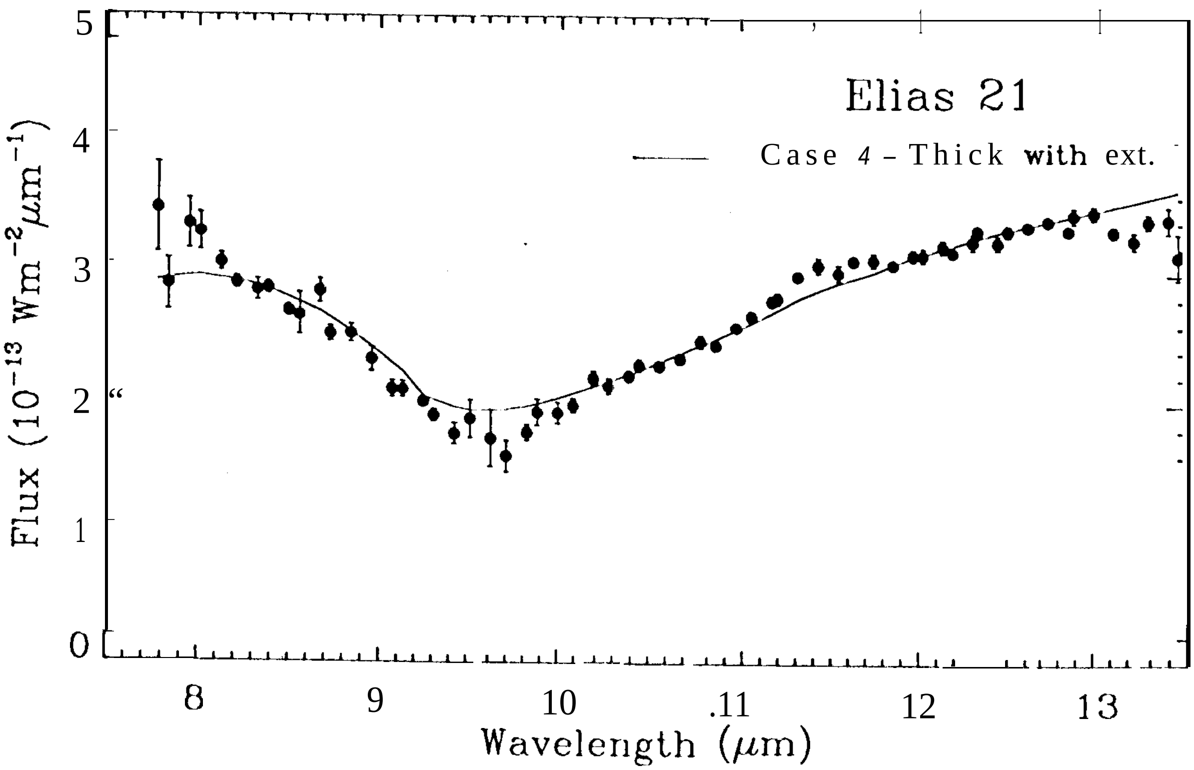
Elias 21
Case 4 - Thick with ext.
Flux (10^{-13} Wm^{-2}μm^{-1})
Wavelength (μm)

Fig 5a, 5b

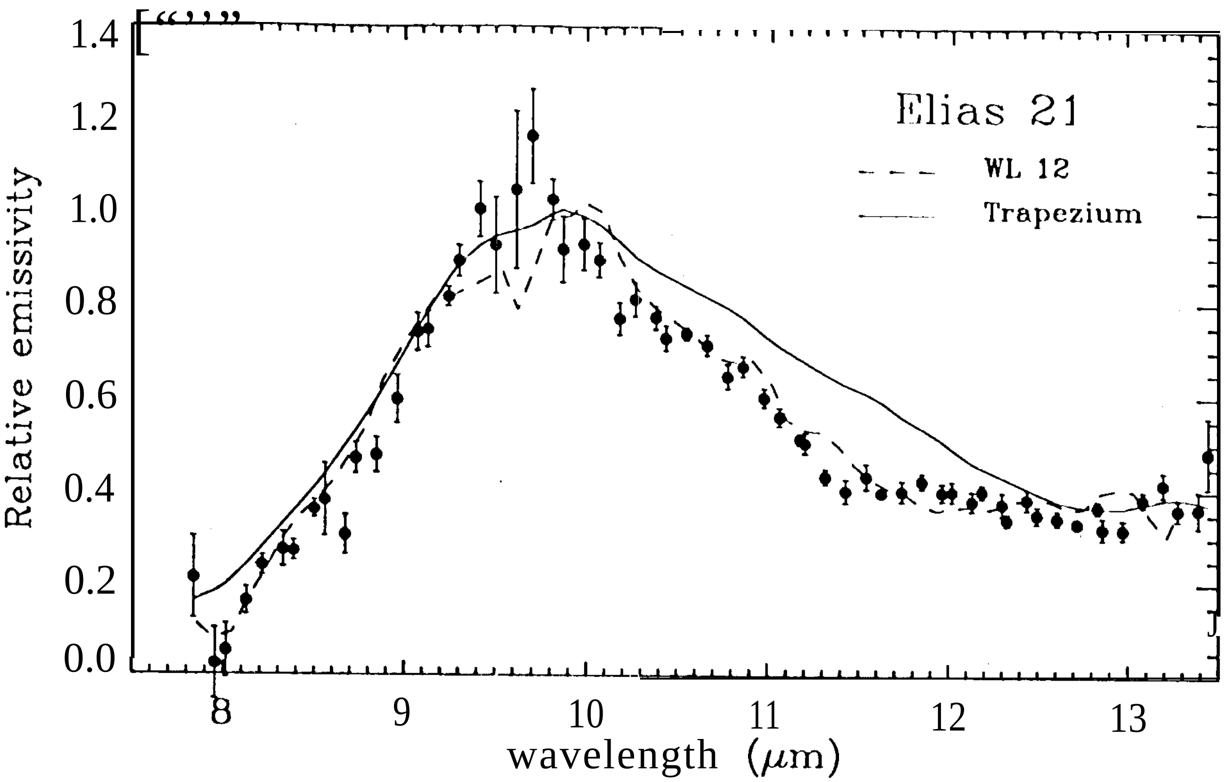
Elias 21
WL 12
Trapezium
Relative emissivity
0.0
0.2
0.4
0.6
0.8
1.0
1.2
1.4
8
9
10
11
12
13
wavelength (μm)

Fig. 6

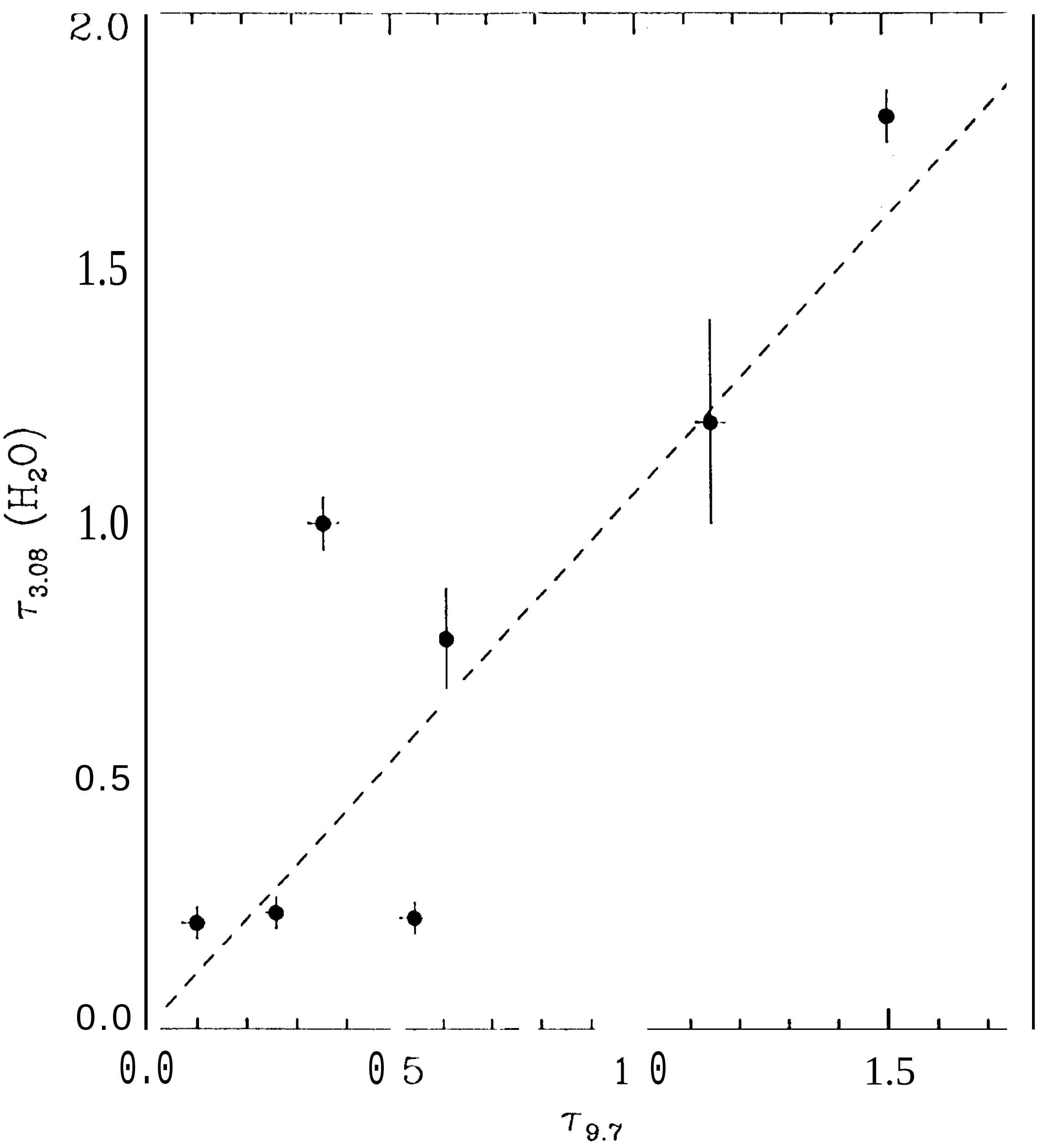

Fig 7